Title

Flexible Long-Reach Robotic Limbs Using Tape Springs for Mobility and Manipulation

Journal

Journal of Mechanisms and Robotics, 15(3)

ISSN

1942-4302

Authors

Quan, Justin

Hong, Dennis

Publication Date

2023-06-01

DOI

10.1115/1.4062150

Peer reviewed

Flexible Long-Reach Robotic Limbs Using Tape Springs for Mobility and Manipulation

Justin Quan* **Dennis Hong**
Robotics and Mechanisms Laboratory (RoMeLa)
Department of Mechanical and Aerospace Engineering
University of California Los Angeles
Los Angeles, CA, 90024
Email: justinquan@ucla.edu, dennishong@ucla.edu

Conventional mobile robots have difficulty navigating highly unstructured spaces such as caves and forests. In these environments, a highly extendable limb could be useful for deploying hooks to climb over terrain, or for reaching hard-to-access sites for sample collection. This paper proposes a new form of multimodal mobile robot that utilizes a novel tape spring limb named EEMMMa (Elastic Extending Mechanism for Mobility and Manipulation). For mobility, the limb can extend prismatically to deploy grappling hook anchors to suspend and transport the main body, or even serve as legs. For manipulation, the limb can morph its shape to bend around or over obstacles and extend to reach into tight spaces. This can allow the limb to retrieve distant objects, position cameras around corners, or place grappling anchors above an overhang such as a table or cliff. The EEMMMa-1 prototype detailed in this paper can climb ladders and shelves in 1.5 bodylengths per second, and can bend up to 100°. A simplified model of the bending kinematics is developed and verification experiments are discussed. The paper concludes by detailing potential applications and configurations of future EEMMMa robotic systems.

Nomenclature

R	Transverse radius (when straight), Fig. 3a
l	Tape spring length, Fig. 3a
t	Tape spring thickness, Fig. 3a
α	Subtending angle of arc swept by tape, Fig. 3a
R_f	Longitudinal radius of localized fold, Fig. 3a
M	Applied external moments, Fig. 3b
θ	Bending angle of fold, Fig. 3b

1 Introduction

Many environments are still difficult for modern mobile robots to traverse, such as cave systems and forest canopies. These have highly irregular features in all directions like stalagmites, cliffs, tunnels, branches, and vines that can make navigation difficult for wheeled or flying vehicles. To safely move through these environments, legged climbing is one method that can offer the required terrain adaptability and safety. Spider monkeys are a good example of a legged creature that is well adapted to movement in complex environments. They suspend themselves in forest canopies using

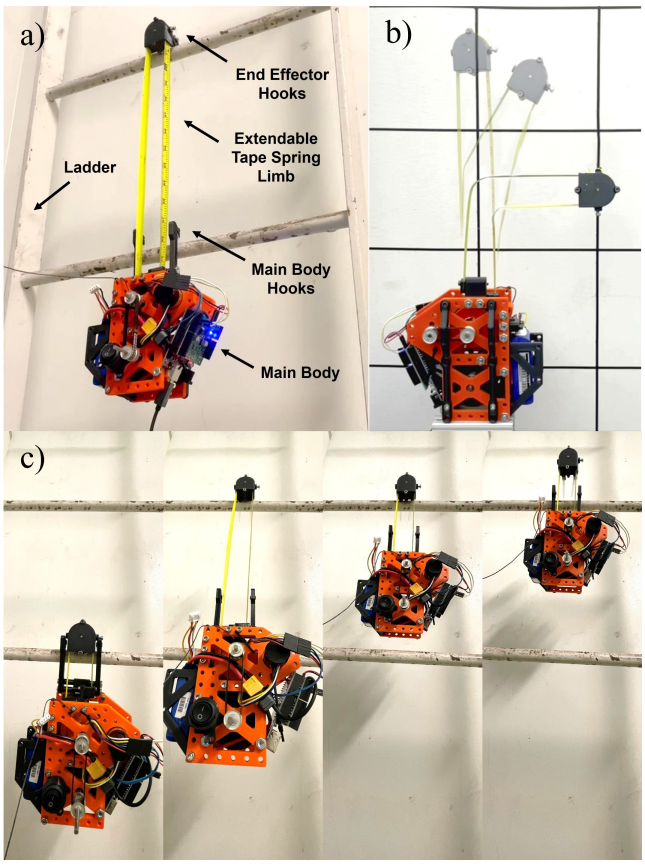

Fig. 1: a) EEMMMa-1 overview, with main body and tape spring limb. The limb can extend to place the end effector hooks on the next ladder rung, allowing it to climb vertically. b) The limb can both extend and bend using a single motor, achieving 2-DOF with a form of mechanical multiplexing. c) Snapshots of the climbing sequence, which can be repeated to scale the entire ladder.

*Address all correspondence to this author.

Fig. 2: Examples of spider monkey suspension during brachiation, using both limbs and tails to grasp multiple points in the forest canopy for enhanced stability while moving. [1]

not just their limbs, but also their tails, depicted in Fig. 2. This gives them an additional anchoring point for safety and allows them to climb swiftly and reach for food with better stability [2].

Many current climbing robots are designed with applications such as surveillance or inspection in mind. There are a wide variety of mechanical approaches to climbing. The simplest type are wheeled climbing robots [3] [4] [5] that can drive vertically but only along flat surfaces. Legged systems adhere to walls using microspines [6] [7] [8], gecko adhesives [9], and even suction cups [10].

These examples reveal important attributes for successful climbing. Most climbing robots are preferably small and lightweight, since they must be able to support their own weight while navigating terrain. Additionally, redundancy is essential for safety, with multiple limbs or anchors to prevent the system from falling if an anchor fails. Finally, legged systems offer much greater adaptability for surface variations, but result in slow speeds and greater complexity since each step must be planned carefully. It should be noted that the movement capabilities of legged climbing robots are limited by the length of their limbs. This limits their range of suitable grappling points, resulting in sluggish systems that require substantial planning time and careful limb coordination.

These systems could be significantly enhanced by utilizing a long-reach extendable limb, greatly simplifying the climbing process by traversing long distances in a single step. This method takes inspiration from grappling hooks and fishing hooks, which involve launching an anchor some distance and reeling it in with a spooled material such as string or rope. While these systems offer long reach in a lightweight and compact package, they lack precision due to the string's amorphous nature. This can be remedied by using a spooled material that naturally holds its shape, like the common tape measure. The tape measure belongs to a class of mechanisms known as tape springs that exhibit natural directional stiffness and can fold for different properties. Utilizing tape springs, grappling hooks can be placed at precise locations from long distances.

This paper proposes a novel form of multimodal mobile robot that uses extendable tape spring limbs for both mobility and manipulation tasks named EEMMMa (Elastic Extending Mechanism for Mobility and Manipulation). EEMMMa's unique tape spring structure allows it to serve as a versatile, lightweight, long-reach limb. For mobility, the limb can extend prismatically to deploy grappling hook anchors to suspend and transport the main body, or even serve as legs. For manipulation, the limb can morph its shape to bend around or over obstacles and extend to reach into tight spaces. This can allow it to retrieve distant objects, position cameras around corners, or place grappling anchors above an overhang such as a table or cliff. Additionally, the tape's elastic properties enable it to self-correct from perturbations for tasks that require alignment. The limb is also safe to use for manipulation tasks since it can simply elastically deform during a collision or if a target is missed.

Figure 1a shows the EEMMMa-1 prototype, a lightweight multimodal single degree of freedom (DOF) robot that uses an extendable tape spring mechanism to demonstrate promising mobility and manipulation capabilities. EEMMMa-1 can climb shelves and ladders using compliant hooks, and can ascend rough vertical walls when equipped with microspines. The extendable limb can also morph its shape with a form of mechanical multiplexing. Using a simple braking function, the limb's kinematics can be changed to control a second rotational DOF using a single motor, allowing the limb to bend as seen in Fig. 1b. A summary video of its capabilities is available in Appendix A.

Section II outlines the overall design and operation of the prototype. Section III shows demonstrations of mobility and manipulation tasks. Section IV analyzes the system's behavior during climbing and bending, outlines a kinematic model, and details experiments performed to validate the model. Section V summarizes the implications of this system and outlines future concepts that can utilize EEMMMa.

2 Design and Implementation

EEMMMa-1's design will be broken down into five main parts: 1) background information, 2) an overview of operations, 3) the tape spring which forms the main structure of the extendable limb, 4) the main body containing the motorized spool, tension management subsystems, and electronics, and 5) the end effector that serves as the end of the limb, and has a braking function for shape morphing.

2.1 Background

Tape spring mechanisms are curved thin shells of material that have the ability to elastically deform and transition between a straight configuration and a folded configuration as depicted in Fig. 3a. In this way, localized "folds" serve as revolute joints, while unfolded straight segments can serve as links that can withstand significant forces in tension, as well as limited compression forces and bending moments. The rigidity exhibited by unfolded segments can be attributed to their transverse curvature, which increases the energetic cost of bending longitudinally [13] [14].

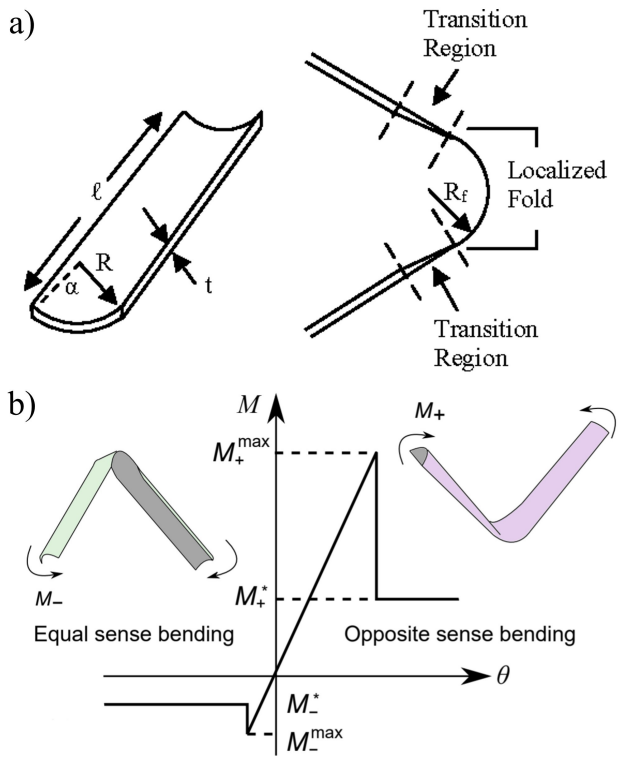

Fig. 3: a) Geometric parameters that define tape springs. An unfolded tape segment is shown on the left, with a locally folded segment on the right. [11] b) Moment-rotation characteristics of 2D folding. [12]

The benefits of tape spring mechanisms have been previously explored in a variety of fields, but there has been little prior work on utilizing the long range of such mechanisms for mobility or manipulation. Tape springs are used in deployable space structures, including extendable booms [15], automatically deploying solar reflectors [16] [17], and large closed-loop structures [18]. A notable example is a planar 3 DOF manipulator for UAVs, which utilizes the long reach of the tape to deploy an end effector below a UAV. This design utilizes a mechanical node that travels along the tape's length to "pinch" and induce a fold to control the bend location and angle [12]. Other applications focus on shape morphing by controlling the locations of the folds and rigid segments. One example utilizes a closed-loop tape to form a 4-bar linkage, utilizing shape memory alloys as actuators [11]. A final example is a cylindrical mobile robot that uses closed-loop tapes to move like an amoeba by everting its compliant body [19].

Tape springs exhibit several useful features for serving as flexible or structural members. When a moment is applied, tape spring segments will not fold until a peak moment is reached. As depicted in Fig. 3a, this localized fold exhibits zero transverse curvature and a uniform longitudinal curvature. If the peak moment is exceeded, the tape spring will exhibit a snap-through buckling behavior with a sudden change in stiffness properties at the fold as it is formed. Additionally, because of the directionality of the tape's curvature, the value of the peak moment changes depending on the direction of the applied moment. As depicted in Fig. 3b, tapes subjected to "equal-sense" bending will fold much more easily than

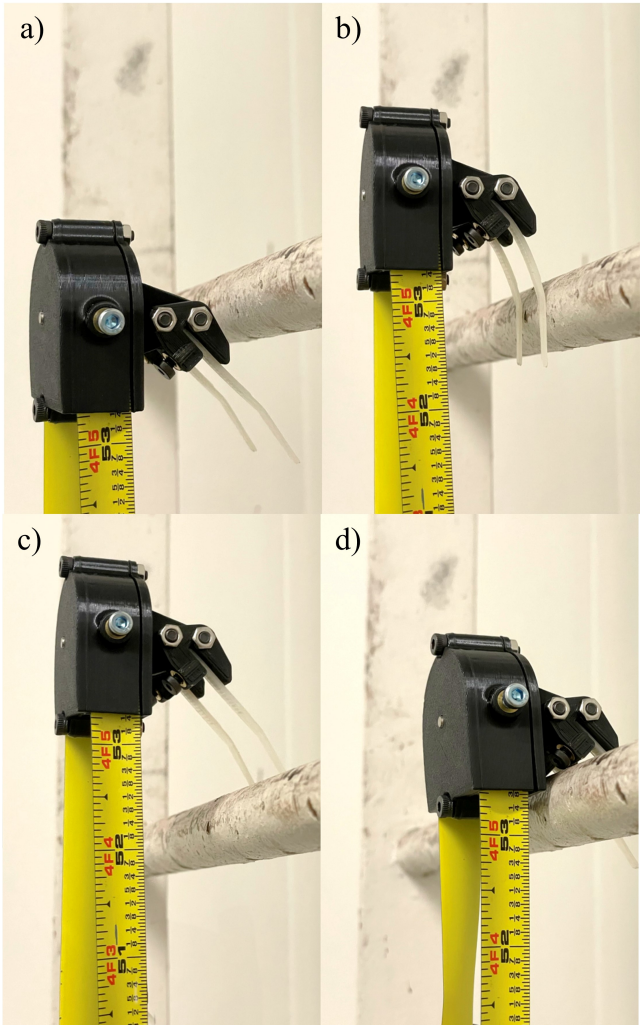

Fig. 4: Sequence of operations for the compliant hooks. a) The hooks approach the underside of the rung. b) The hooks contact the rung and begin deforming as they continue to rise. c) The hooks pass the rung, and the compliant tips spring to their original shapes. d) The hooks are lowered onto the rung. The reaction force from the angled surface pulls the assembly towards the rung until it settles at the root of the hook, creating a sturdy anchor point.

for "opposite-sensed" bending [20]. The development and propagation of folds is highly dependent on the loading and boundary conditions present at the end sections of the tape spring [21]. Tape springs also exhibit a level of self-actuation due to their spring properties, which will cause the tape to elastically return to its unfolded neutral state when bent or twisted [22].

2.2 Overview of Operations

Designed primarily to demonstrate climbing on shelves and ladders, EEMMMa-1 is equipped with two sets of compliant hooks to climb successive levels, as seen in Fig. 1c. The first set of hooks is located on the main body and serve to anchor the main body at the current shelf or ladder rung. The second set of hooks is attached to the end effector.

The hook engaging sequence can be seen in Fig. 4. As the tape extends vertically, the end effector hooks gently deform to allow them to pass above the next level. The hooks

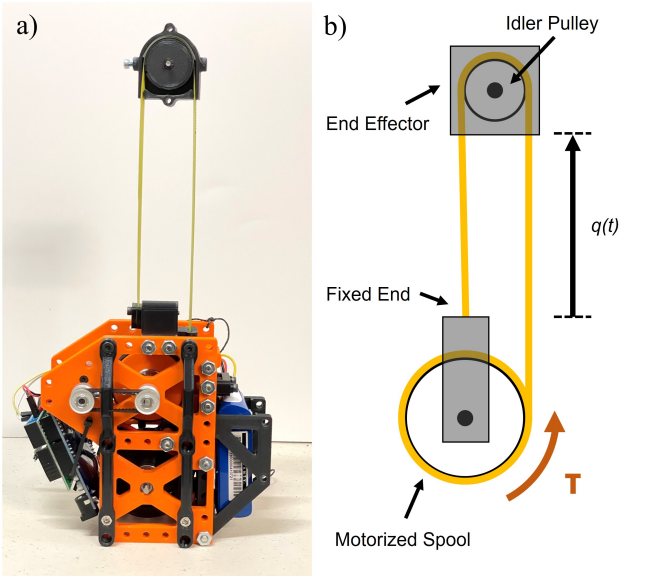

Fig. 5: Overview of EEMMMa-1's tape mechanism. a) The prototype in basic prismatic configuration, with end effector casing removed to show the continuous U-shaped tape path. b) Diagram of the tape path, with the extended length $q(t)$ as the input variable.

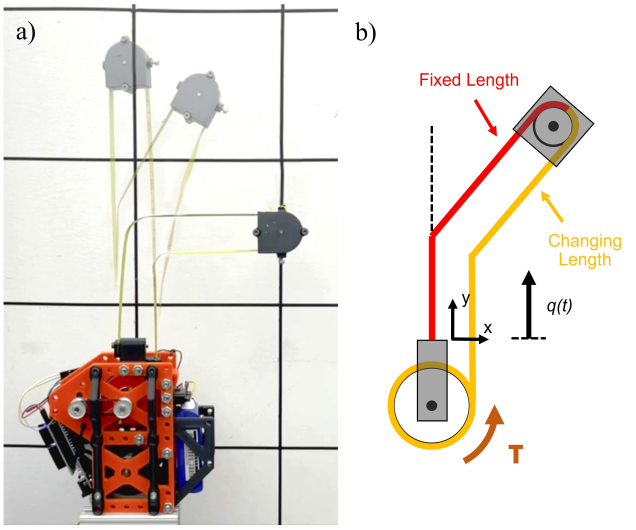

Fig. 6: a) Overlaid snapshots of the bending sequence, deployed vertically and bending in the Z-axis. b) Diagram of the internal tape path in "brake" mode. The input $q(t)$ now controls only one side of the tape, and the resulting difference in segment lengths causes the limb to rotate until a fold is generated.

then spring back to their original positions after they clear the level, resulting in a one-way locking effect. As the main body reels itself upwards, the sloped hooks passively guide the shelf or ladder rung onto the load-bearing back portion of the hook, establishing a new anchor point. Once the main body hooks pass the next level and establish stable contact, this grappling and anchoring sequence can be repeated.

The overall weight of the system is 685 grams, consisting of a 640 g main body, 35 g end effector assembly equipped with hooks, and 10 g of steel tape. Much of this weight comes from excess fasteners and components included for adjustability and modularity that can be removed in future designs.

2.3 Tape Spring Limb

The tape provides the main structure for the limb, and is stored in a spool in the main body. It is folded into a U-shape as seen in Fig. 5b. In the U-shaped bend, an idler pulley passively follows the traveling fold at the "end" of the limb, allowing the end effector to move up and down. The idler and the U-shaped tape form a pulley system that provides mechanical advantage that halves the torque required to lift the main body while climbing.

The U-shaped tape has one end connected to the spool and the other end fixed to the main body,with the transverse curvature pointing outward. This layout essentially creates three tape regions: two unfolded segments placed back-to-back, and a folded segment connecting that makes up the bend of the U. When tape springs are placed back-to-back, the overall structure exhibits significantly improved stiffness, since one of the tapes is subjected to opposite sense bending regardless of bend direction [23] [24] [25]. EEMMMa-1 utilizes this advantageous property while only requiring actuation of a single continuous tape. Additionally, the elastic spring properties of the tape assist with maintaining the orientation of the hooks during extension and engagement, resulting in robust climbing capabilities.

EEMMMa-1 can initiate shape morphing using a form of mechanical multiplexing to bend the limb, depicted in Fig. 6. By activating a braking function at the end effector, the system can switch its kinematic mode. The brake locks the end effector relative to the tape's surface by pressing a small rubber pad, creating a local "fixed" boundary condition. Since one segment is "fixed", it will not change length, while the other actuated segment will decrease in length. The disparity in lengths causes the upper half of the assembly to rotate until folds are generated, which serve as revolute joints. This simple on-off braking function allows EEMMMa-1 to bend with minimal added weight, effectively granting the arm 2-DOF capabilities with only a single main motor, although it cannot actuate both DOF simultaneously.

The material used is a uniform segment of pre-stressed steel tape cut from a Pittsburgh brand 12 ft. x ½ in. tape measure, with a 0.006 in. thickness. This tape width of ½ in. is relatively small when compared to 1-¼ in. used in other projects [12] [26]. This results in reduced bending stiffness and limb rigidity, but also lighter weight and easier shape morphing since the peak moment required to induce folds is lower. Since this prototype was designed for climbing, the reduced bending stiffness is inconsequential since the tape is almost always loaded in tension. The tape's total length is 1 m, allowing the limb to extend 50 cm away from the main body. This distance was chosen specifically for climbing ladders, which commonly have rungs with 4 cm diameter, spaced 30 cm apart. Both ends of the tape have 3 mm holes drilled in their centers to rigidly connect to the spool or frame.

2.4 Main Body

The main body forms the primary structure that houses the motorized spool, tension management subsystem, and electronics. These components are placed in specific locations to make the center of mass close to vertically aligned with the tape axis. This is to reduce pitching moments that can disrupt hook alignment while climbing or cause the system to fall [27]. The frame is primarily composed of 3D printed PLA and steel fasteners, and measures 130 x 140 x 95 mm.

The 40 mm diameter spool is surrounded by an outer casing with a small exit hole to confine the coiled tape loops, which will unwind themselves or push out of plane due to instabilities while coiled [28]. The inside of the spool casing is lined with a strip of nylon to reduce friction.

After leaving the spool, the tape enters the tension management subsystem. An output roller covered with non-slip rubberized surface (neoprene) grips the tape as it exits to maintain a tension force inside of the tape that keeps the tape properly coiled around the spool. The spool and roller have the same diameter and are geared 1:1 to ensure the tape deploys smoothly. While this is sufficient for shorter lengths, longer lengths of spooled tape will result in the spool diameter decreasing as more tape is deployed, which may cause tensioning issues for future prototypes.

Finally, the tape exits the main body at the output hole, which has a curved shape that follows the tape's transverse curvature. This is to ensure the tape deploys in an unfolded state for maximum rigidity. When there are disturbances from forces at the end effector, the output hole's curved surfaces reduce the likelihood of a stress concentration which may result in an unwanted fold.

2.5 End Effector

The end effector assembly provides a structure at the end of the limb for mounting any additional mechanisms that interact with the environment such as hooks or cameras. Inside the end effector is the idler pulley, which is wrapped in rubberized tape and is 29 mm in diameter. Folded tapes exhibit a characteristic longitudinal curvature based on the tape's manufacture, which is 29 mm for this tape.

An outer casing surrounds the idler and tape. The inside of the casing contains a small nylon pad at the tip of the fold, which allows the end effector to transfer loads to the tape in both tension and compression with minimal friction. The casing also prevents the traveling fold from splitting into two separate folds when loads are applied.

3 Demonstrations

In the following demonstrations, EEMMMa-1 shows its effectiveness as a multimodal platform for both mobility and manipulation in a lightweight, compact package. By leveraging the tape spring's unique properties, EEMMMa-1 can demonstrate climbing, bending, pushing, and pulling. These tasks require only two parameters to be controlled: the length change of the tape, and the on/off of the end effector brake.

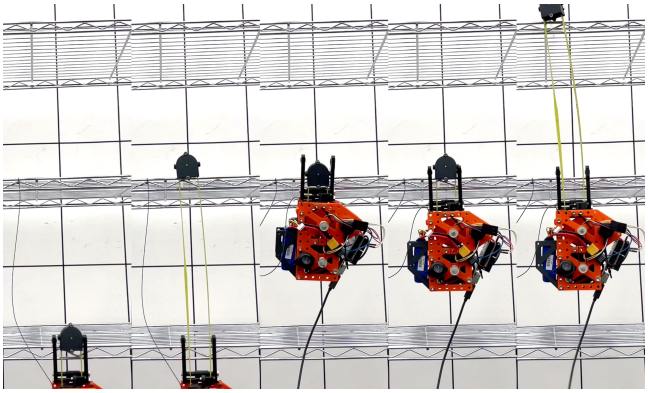

Fig. 7: Snapshots of shelf climbing demonstration.

3.1 Climbing

To verify the limb's ability to handle loads in tension, EEMMMa-1 was subjected to climbing trials in three scenarios: climbing a shelf, a ladder, and a rough vertical wall. Trials were first conducted on wire-frame shelves made of 5 mm diameter wire, seen in Fig. 7. The shelves had a thickness of 22 mm and were spaced 254 mm apart for a total of 276 mm to ascend per level. EEMMMa-1 can ascend at 19 cm/s, traversing a level at top speed in about 2 seconds. This is about 1.5 body lengths per second, which matches that of the fastest wall climbing robots [29]. For ladder climbing trials, straight vertical ladders were used, which are commonly seen in industrial or mechanical environments such as factories, buildings, and ships. The ladder chosen had cylindrical rungs with 2 cm diameter, spaced 28 cm apart for a total of 30 cm to ascend per level. The larger diameter of the ladder rungs caused more significant perturbations from the compliant hooks. When climbing at top speed, these perturbations caused hook alignment issues during multiple climbs in succession, although trials at slower speeds were successful.

For the wall scaling trials, the end effector compliant hooks were swapped with a small microspine array, seen in Fig. 8. This microspine array is composed of four small steel hooks, with sharp points that engage in asperities on the rough surface. Outer housings and rubber bands provide rotational and translational compliance for engagement and load sharing. EEMMMa-1 could successfully cling to the wall and ascend small distances. However, this prototype was unable to perform multiple grappling and anchoring sequences in succession due to two main effects. First, the main body's center of mass being slightly off center caused the body to pitch and the limb to extend at an angle. At large extensions, this caused the end effector microspines to be too far away from the wall to engage the surface properly. Additionally, the microspine array footprint was small enough to be approximated as a point contact, which sometimes caused the anchor to twist off the surface during perturbations. A future body redesign and microspine array upgrade could alleviate these issues.

For all climbing trials, the elastic spring properties of the tape proved to be beneficial for resisting unwanted forces or moments at the end effector. Hooks require directional engagement, and they must approach the grappling features at a

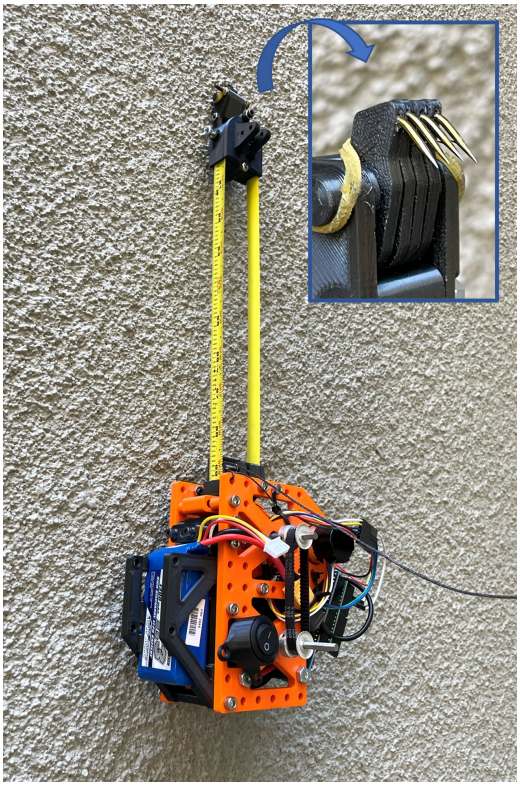

Fig. 8: Snapshot of EEMMMa-1 climbing a rough vertical wall. The end effector's small microspine array grips into asperities in the rocky surface.

specific orientation to be effective. This is especially important for microspines, which can peel away or fail to engage if they are not properly aligned with the gripping surface. These experiments were performed with simple open-loop control and manual input. Because correctional forces are passively supplied by the tape's spring properties, the climbing sequence is robust and simple to control. However, future designs with larger extension lengths and heavier end effectors may experience additional difficulties since the end effector may oscillate over long periods and require long settling times to passively re-establish alignment without added stiffness or damping. These trials demonstrate EEMMMA-1's ability to pull loads against gravity, which is vital for suspending the main body in midair from above, or for retrieving samples from below.

3.2 Bending

Robotic manipulation tasks commonly require reaching a target in space, so the next set of tests were devised to demonstrate EEMMMa-1's ability to reach a desired location on a plane using controlled bending. Since it is trivial to reach any single point along the 1-DOF linear path, trials involved reaching two points on the plane, seen in Fig. 6a. For the first set of trials, the limb was pointed vertically, extending in the direction opposite gravity. This was selected as the most relevant scenario for this system, since climbing actions generally involve vertical movement, and bending would be advantageous for reaching above tables or steps. For the first test, the limb was first extended to point A located 20 cm above the main body at coordinates (0,20) cm. Next, the end

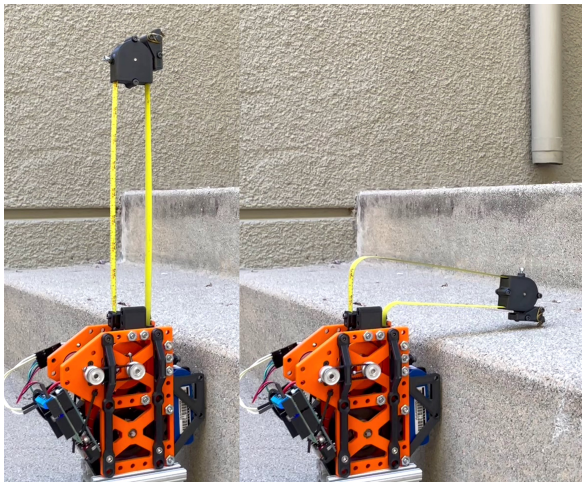

Fig. 9: Snapshots of EEMMMa-1 bending to place a microspine anchor on the top surface of a step.

effector braking system was engaged, allowing the motor to initiate limb bending. Actuation was applied slowly until a fold was created in both tape segments, essentially serving as a new revolute joint. After rotating 90 degrees, the end effector successfully reached point B located at (10,10) cm. Video footage was taken on a gridded background to verify repeatability. The tape's bending kinematics and behavior will be discussed in more detail in Section IV.

Subsequent bending trials to other points in the plane revealed additional phenomena. Angling the revolute joint more than 100 degrees resulted in the folds suddenly migrating towards the main body, causing the limb to "collapse". Limb collapse also occurred when extending the spool to reach most points in the -X direction (see Fig. 6b). This is due to the fixed segment being loaded in equal-sense bending rather than opposite-sense bending, which will cause buckling under a much lower peak moment. It was also found that the location of the fold could be controlled through dynamic inputs, which will be discussed more in Section IV.

As a test application for bending, EEMMMa-1 was placed on a stone staircase to demonstrate anchoring to steps with microspines, shown in Fig. 9. The limb was extended vertically above the next step, and a fold was induced to angle the end effector downwards.The limb was intentionally actuated to generate the fold close to the base instead of the midpoint to allow the hooks to contact the ground. The tape was then retracted slowly, allowing the spines to fully engage and pull the body in. Tests revealed that the tape's natural spring properties assist with maintaining the proper spine orientation during all phases of movement, including approach, engagement, and retracting. These tests demonstrate the potential for EEMMMa to serve as a long reach, low complexity manipulator arm that can bend around or over obstacles to position grippers, cameras, or other instruments in difficult to reach places.

3.3 Standing

A simple "standing" test was performed as a demonstration of the limb's ability to handle loads in compression by

Fig. 10: EEMMMa-1 standing demonstration. The limb is deployed downward, with the end effector secured in a vice. The weight of the main body loads the limb in compression, similar to a weight-bearing leg.

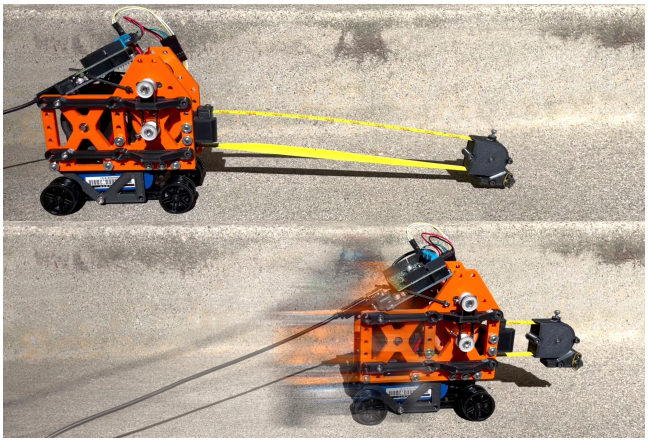

Fig. 11: Snapshots of EEMMMa-1 crawling demonstration, equipped with passive wheels.

serving as an extendable prismatic leg, as seen in Fig. 10. First, the end effector was placed in a vice with the main body carefully positioned directly above. The limb was extended and the main body was released, with its weight creating a compressive load on the limb. These static loading tests were successful up to 20 cm of limb extension. Beyond this point, the limb's rigidity was insufficient to prevent small perturbations from causing the body's center of mass to shift, which resulted in a collapse. Dynamically extending the limb also caused collapses at longer lengths, since reaction moments at the main body resulted in the center of mass shifting and would cause the system to topple over.

These tests demonstrate the end effector's effectiveness at allowing the limb to handle compressive loads. Because the tape is a single continuous U-shape, loads can be transferred evenly between the two opposing segments. The end effector housing effectively confines the U-shaped tape fold without it splitting or propagating, which would result in a greatly reduced ability to handle loads as a manipulator. The ability to successfully handle compressive loads is promising for future EEMMMa designs, which will feature multiple limbs and not exhibit the same collapsing issues due to load sharing between the limbs.

3.4 Crawling

As an additional test for mobility, EEMMMa-1 was equipped with passive wheels on the underside of the main body to demonstrate 1-DOF crawling along the floor, depicted in Fig. 11. The end effector was equipped with the microspine attachment and the limb was extended. When outstretched, gravity causes the limb to sag slightly, allowing the end effector microspines to contact the floor. The tape was retracted slowly to engage the microspines, then a fast retraction pulled the body forward. The main body would then coast linearly on the floor, carried by momentum. As the body approaches the end effector, the microspines would naturally disengage due to the changing angle of engagement. This demonstrates EEMMMa's ability to be used with other mobility schemes, and operate with them in combinations for various effects. For example, this could be useful if a rover lost power to its wheels, but could still operate using its EEMMMa manipulator arm for mobility.

4 Analysis and Discussion

4.1 Bending Behavior

The limb's ability to extend and bend in a controlled, repeatable fashion can be explained by analyzing the tape's properties. From previous work, the bending stiffness of a tape segment can be characterized by its material and four geometric parameters: its unstressed radius of curvature R, thickness t, subtended angle α, and length ℓ, as previously depicted in Fig. 3a.

Snapshots from the bending trials are shown in Fig. 12 displays three stages of behavior that the limb exhibits as it bends from 0° to 90°. Under normal 1-DOF operation, the tape operates as a single continuous piece of material, moving the end effector as the idler pulley rolls along the tape's length. Activating the brake at the end effector functionally separates the tape into two segments, S_1 and S_2. The actuated segment S_1 on the right is attached to the spool, and has a variable length that can be changed by actuating the motor. The segment S_2 on the left now has a fixed length due to its end attachment to the main body. By retracting the tape, S_1's length is reduced, and the end effector begins to rotate due to the disparity in lengths. As the bending angle increases, the limb goes through the three stages of bending behavior

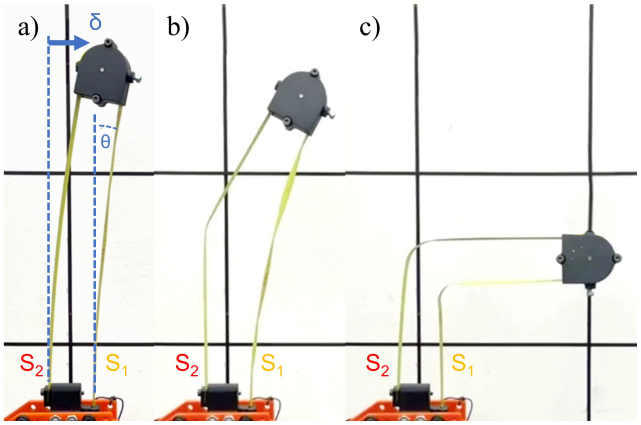

Fig. 12: Three stages of behavior for bending. a) For small angles ($0° < \theta < 10°$), both segments are unfolded, and displace some distance δ. b) For medium angles ($10° < \theta < 40°$), S_2 has a fold while S_1 is unfolded, but experiences combined twisting and bending. c) For large angles ($40° < \theta < 90°$), both segments are folded, creating two revolute joints.

as follows:

Stage 1: S_1 and S_2 are both unfolded and behave like beams.
Stage 2: S_2 has a fold, S_1 is unfolded but bends and twists.
Stage 3: S_1 and S_2 both have folds which each behave like a revolute joint.

In Stage 1, depicted in Fig. 12a, both tape segments exhibit small horizontal displacement. S_2 is subjected to opposite-sense bending, and it can be treated as a single flexible beam until buckling occurs. By treating this case as a beam deflection, the applied moment can be calculated:

$$M = \frac{2\delta EI}{S_2^2} \tag{1}$$

where δ is the tip displacement of S_2, E is the elastic modulus of the tape material, I is the second moment of area of the cross section. For an unfolded tape, I can be found using the geometry of the curved cross section:

$$I_u = \frac{R^3 t}{2\alpha}[\alpha^2 - 4(1 - cos(\alpha)) + \alpha sin(\alpha)] \tag{2}$$

S_2 exhibits linear behavior until the applied moment exceeds the peak moment M_+^{max} and a fold is created (see Fig. 3b). Meanwhile, S_1 is subjected to equal-sense bending, and will bend and twist simultaneously until the negative peak moment M_-^{max} is reached and a coherent fold is formed. This flexural-torsional deformation mode is difficult to capture mathematically, but equations governing this behavior and peak moments were derived in Seffen's work [23]:

$$M_+^{max} = (1+\nu)D\alpha \tag{3}$$

$$M_-^{max} = (1-\nu)D\alpha \tag{4}$$

$$D = \frac{Et^3}{12(1-\nu)} \tag{5}$$

where ν is Poisson's ratio of the tape material.

In Stage 2 (Fig. 12b), the fixed segment S_2 has folded while the actuated segment S_1 has not, but continues to experience combined bending and twisting. When folded, the curve flattens and the cross section becomes rectangular. The required applied bending moment of the flattened tape is:

$$M = EI_f\kappa = ER\alpha\frac{t^3}{12}\kappa \tag{6}$$

$$I_f = R\alpha\frac{t^3}{12} \tag{7}$$

where κ is the longitudinal beam curvature and I_f is the second moment of inertia for the folded tape. Note that the formulation of I changes significantly due to the change in cross section, which now exhibits a much lower stiffness for rotations about the Z axis.

Folds will generally occur at the midpoint of segments, since the loads at the ends are equal and opposite. Due to this symmetry, the fold will not propagate or travel along the tape's length, assuming minimal effects from external forces. Since the fold is symmetric and located away from endpoints, it can be modeled as a point hinge [20], simplifying our analysis. In this stage, S_2 behaves as two rigid segments connected by a revolute joint, while S_1 behaves nonlinearly as a beam undergoing large deflection, with higher flexural-torsional deformation that can be characterized using Mansfield's equations [30].

In Stage 3 (Fig. 12c), both segments have folded at their centers, essentially creating a new revolute joint for the limb. The limb can easily be returned to the straight prismatic configuration by equalizing the lengths. This is partially assisted by the tape itself, which will attempt to straighten in order to relieve the accumulated strain energy from bending [20].

4.2 Two Dimensional Bending Kinematics

Figure 13 shows the parameters that define the 2D kinematics for this vertically deployed limb at large bending angles. The forward kinematics of the end effector at point C can be defined in terms of virtual link length L and bending angle θ:

$$x = -Lsin(\theta) \tag{8}$$

$$y = L + Lcos(\theta) \tag{9}$$

The limb consists of two virtual links: the first link goes from the midpoint of the base A to the center point between

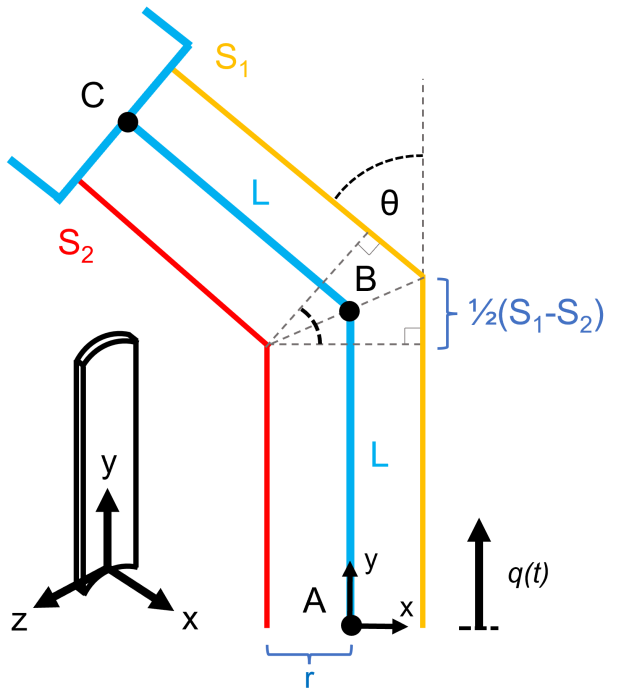

Fig. 13: Limb bending kinematics. The state of the two opposing segments of tape S_1 and S_2 determine the state of the virtual links L in blue that approximate the overall limb.

the two tape folds B, and the second goes from point B to the center of the pulley C. Since end loads of the two tape segments are symmetric about point B, both of their bends will occur at the midpoint of the segments. Thus, both links AB and BC have equal length L, which is dependent on the lengths of the right actuated segment S_1 and left fixed segment S_2. The bending angle theta is defined as the angle between the two virtual links, which is dependent on the difference between S_1 and S_2. The two tapes are parallel and offset by a distance r from the centerline, which is the radius of the end effector idler pulley (and also characteristic bending radius of the tape). Since L is located at the center between the two tapes, we can use triangle similarity rules to draw two conclusions:

$$L = \tfrac{1}{4}(S_1 + S_2) \tag{10}$$

$$tan(\frac{\theta}{2}) = \frac{\frac{1}{2}(S_1 - S_2)}{2r} \tag{11}$$

Both of these values are dependent on S_1 and S_2, which are determined by our single control variable $q(t)$, which is the length of tape extended/retracted from the base. However, the braking function gives us two modes for formulating S_1 and S_2. In "free" mode, the braking function is off, a change of $\dot{q}(t)$ will result in S_1 and S_2 changing lengths equally. In this case, lengths $S_1(t)$ and $S_2(t)$ are given by:

$$\begin{bmatrix} S_1 \\ S_2 \end{bmatrix} = \begin{bmatrix} \frac{1}{2} \\ \frac{1}{2} \end{bmatrix} q(t) + \begin{bmatrix} S_1(0) \\ S_2(0) \end{bmatrix} \tag{12}$$

where $S_1(0)$ and $S_2(0)$ are the lengths of the tape segments at time $t = 0$. However, when in "brake" mode, only S_1 changes length while S_2 remains fixed at its initial length.

$$\begin{bmatrix} S_1 \\ S_2 \end{bmatrix} = \begin{bmatrix} 1 \\ 0 \end{bmatrix} q(t) + \begin{bmatrix} S_1(0) \\ S_2(0) \end{bmatrix} \tag{13}$$

It can be observed that the two kinematic modes determine how theta is formulated. In the "free" mode, computing the $S_1 - S_2$ term results in $q(t)$ canceling out. This means that the theta is not dependent on $q(t)$ and will be unaffected by extending/retracting the tape. However, in "brake" mode, the $q(t)$ term reappears in theta and can now be controlled by inputs. Substituting either of these Equations into Equation 1 yields the system:

$$\begin{bmatrix} x \\ y \end{bmatrix} = \frac{1}{4}\begin{bmatrix} -sin(\theta) \\ 1 + cos(\theta) \end{bmatrix} q(t) + \frac{1}{4}\begin{bmatrix} -sin(\theta) \\ 1 + cos(\theta) \end{bmatrix} [S_1(0) + S_2(0)]$$

4.3 Experimental Validation

To analyze the accuracy of the formulated bending kinematic equations, a series of tests were conducted to compare the actual end effector position with calculated theoretical values during bending. To collect position data, the end effector was outfitted with a colored marker that was tracked real-time via webcam. The collected position data was then mapped from pixel space to actual X-Y position in meters. For each experiment, the tape spring limb was extended to a set initial length ($S_1(0)$ and $S_2(0)$ set to some value). Bending mode was initiated, and the spool was commanded to slowly retract a set distance ($q(t) < 0$) until the limb reached $-90°$, with the end effector moving along a curved path through the first quadrant of the X-Y plane.

Figure 14 shows a selection of data points from multiple bending trials at two different initial lengths. Predicted values are overlaid as solid lines, which were calculated using the kinematics equations outlined in the previous section. For the first trial, the limb was extended to 27 cm before bending. This distance is half the total extension length and is a good representation of the limb's average behavior. In the second trial, the limb was extended to 14 cm before bending to show behavior at smaller extensions. Additionally, the limb was tested at greater extensions (above 40 cm) but the limb would frequently collapse after bending more than $-45°$ due to the greater sensitivity at long extensions. Slight vibrations would cause uncontrolled fold migration and limb collapse, leading to inconsistent results, so they are omitted for this study.

For these randomly selected data points, there is a small amount of variance in the measured positions between trials. This is likely due to a combination of minor factors, including slight disturbances from vibrations, tracking errors from the camera, and slightly different starting conditions caused by backlash and friction in the spool.

Figure 15 shows 4th order polynomial trendlines for the collected data compared to the predicted values. These

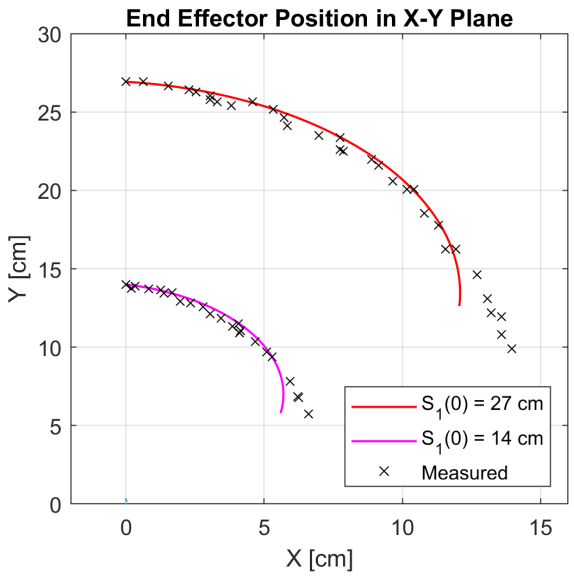

Fig. 14: Comparison of predicted end effector positions vs actual measurements over multiple trials for bending from $0^\circ < \theta < -90^\circ$. Two sets of data are shown for an initial extended length of $S_1(0)$ = 27 cm and $S_1(0)$ = 14 cm. Predicted values are represented by the continuous lines.

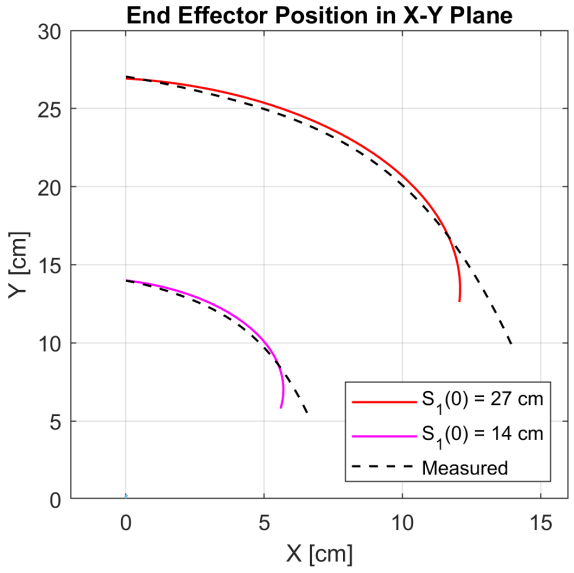

Fig. 15: Comparison of predicted end effector positions versus trendline for actual measurements.

graphs show that the model tracks well from $0^\circ < \theta < -70^\circ$. For a given angle, the model deviates from the actual X-Y position by no more than 3% for both trials. Bending beyond this region causes the actual data to deviate significantly from the model's prediction.

These deviations can be explained by the effects of gravity and folding, which are not accounted for in the previously described model. Gravity has a significant effect on the motion, since the weight of the end effector generates an additional torque on the tape spring segments. This causes the end effector to sag slightly in -Y, just below the predicted position. The weight also appears to change the fold location when bending at angles beyond -70°, causing the fold to

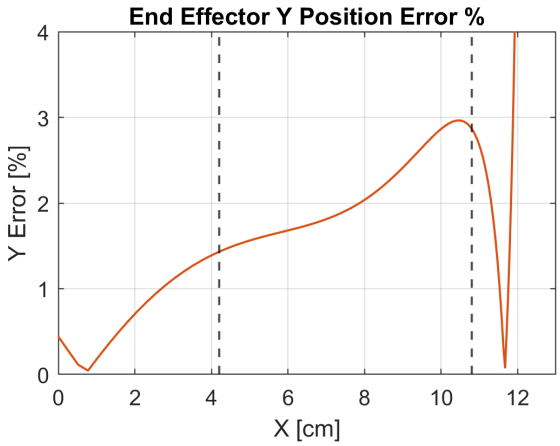

Fig. 16: Y Position error between the predicted path and the measured value trendline for the 27 cm trials. The vertical dashed lines at X = 4.2 and 10.8 cm depict the transition points between the three stages of bending previously shown in Fig. 12.

migrate away from the midpoint. Since the kinematic equations were formulated with the assumption that the fold is always at the tape segments' midpoints, the end effector's actual position begins to deviate significantly from the model. It should be noted from Fig. 14 that the fold migration appears to be predictable, since the end effector traveled along the same approximate path between separate trials.

To better study these effects, Fig. 16 shows the error in Y position between the predicted path and the trendline for the measured data for the 27 cm trials. As the end effector moves further in the +X direction, we can see the effects of the three stages of bending previously shown in Fig. 12. The vertical dashed lines at X = 4.2 cm and X = 10.8 cm separate the graph into the three bending stages as observed from captured test footage.

In Stage 1 ($0 < X < 4.2$), neither tape segment has a coherent fold. The end effector's weight is still supported by the mostly vertical tape segments, so it does not cause much sagging and the error remains relatively low.

In Stage 2 ($4.2 < X < 10.8$), one of the tapes has folded, which dominates the end effector's kinematics. However, the newly generated fold also causes the folded segment to have reduced rotational stiffness. The weight from the end effector also contributes a growing amount of external torque since its moment arm increases as it moves further in +X, which causes the error to increase.

In Stage 3 ($X > 10.8$), both segments have formed folds, but the fold migration appears to take effect. The fold migration changes the kinematics of the system and causes the Y position to drop much faster than expected. After intersecting with the predicted path, the error increases rapidly as the end effector follows a new path. Additionally, the sagging effect from the end effector weight is much more pronounced due to its large +X distance, as well as from the decreased rotational stiffness of both tape segments.

The fold migration is most likely caused during the physical transition from Stage 2 to Stage 3. The sudden formation of the fold causes a significant disturbance to the system as the tape snaps through to its new configuration. While

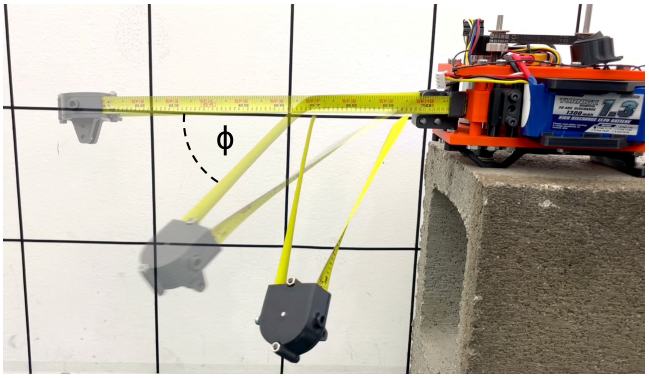

Fig. 17: Demonstration of out-of-plane bending, where the applied bending moment is perpendicular to the moment from the end effector's weight.

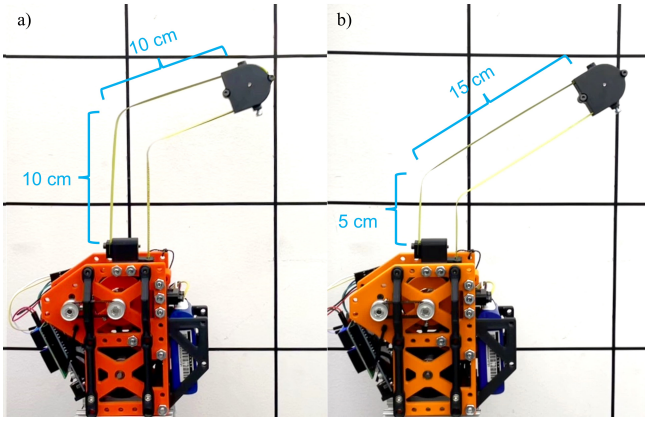

Fig. 18: Example of the fold location changing from dynamic input. a) Base case where slowly actuating causes the fold to occur at the tape midpoints. b) Dynamic case where actuating in dynamic bursts causes the fold to occur at a different location.

outside the scope of this paper, the kinematics model should be improved in future studies to compensate for the effects of gravity and fold migration.

4.4 3D Bending and Dynamic Input Investigations

In the bending experiments outlined above, all end effector movement occurs in the 2D X-Y plane only. This is because the tape is deployed vertically. Actuating the spool in this configuration applies a bending torque about the Z-axis, and the weight of the end effector generates a torque that is also about the Z-axis. Thus, all rotations and forces cause movement in X-Y only and the system remains in a single plane.

However, when the tape is deployed horizontally as depicted in Fig. 17, inducing a fold can cause the limb to bend out-of-plane, resulting in a 3D fold. This is because actuating the spool applies a torque about the Y-axis, but the moment arm from the weight of the end effector causes a rotation about the Z-axis. In this case, the fold will exhibit both bending and twisting in θ and ϕ. Since ϕ is a function of the Z-axis moment arm, it can be controlled by simply extending the tape. This method allows effective control of the end effector's out-of-plane displacement until the peak moment is reached and the limb collapses. Future versions of EEMMMa can potentially use this phenomenon to grant the limb 3-DOF without another actuator, taking advantage of gravity to achieve out-of-plane movement.

Additional tests show that the limb can be manipulated in even more ways if dynamic inputs are used. In preliminary tests, the tape was retracted in short bursts, resulting in oscillations at the end effector. If the tape was retracted again before the oscillations settled, the fold location could be altered depending on the state of the end effector, depicted in Fig. 18. The timing of these actuation bursts can also potentially be used to minimize oscillations at the end effector by cancelling out vibrations with well-timed retractions. This phenomenon has been observed in previous tape spring studies where the fold travels due to impulse-momentum interactions [20] where the tape is modeled as a traveling hinge with hinge position and rotation angle as two independent degrees of freedom.

While analyzing and controlling these additional degrees of freedom are outside the scope of this paper, these phenomena are important to note for their potential to enhance EEMMMa's available workspace and manipulation capabilities in the future.

5 Conclusion and Future Work

This paper introduced the novel concept of utilizing tape spring mechanisms for robotic limbs that can serve for dual mobility and manipulation tasks. Tape springs exhibit unique characteristics that can be valuable for a robotic limb, such as compact retractability, long reach, simple construction, elastic self-correcting, and safety. The EEMMMa-1 prototype presented in this paper demonstrates the powerful versatility of a single EEMMMa limb, providing key functions such as climbing and bending with only one actuator.

Future mobile robots can utilize combinations of EEMMMa limb configurations and end effectors to achieve a wide range of mobility schemes. The EEMMMa-2 climbing robot is currently under development. EEMMMa-2 will be a two-limbed, 3-DOF planar manipulator equipped with microspines for anchoring into rough walls. EEMMMa-2 will be able to grasp parallel walls to suspend itself in midair by aiming and deploying anchors, then simultaneously reeling in both limbs.

The long term goal envisioned for this project is a lightweight three or four-limbed robot that can move in 3D space by aiming and anchoring onto different locations with its extendable limbs, depicted in Fig. 19a. From its suspended position, it can then reel itself in or even swing to transport itself quickly. Since this mobility scheme only requires three anchor points for safe motion, this system would be excellent for navigating through caves or dense forests where terrain is highly unstructured and there are large vertical structures for anchoring and climbing. For a three-limbed system, since only two limbs are needed to suspend the body, the third limb could be used to deploy a camera or retrieve a sample from below. For a four-limbed system, the multimodal nature of each limb grants the system built-in redundancy for both mobility and manipulation tasks. Even

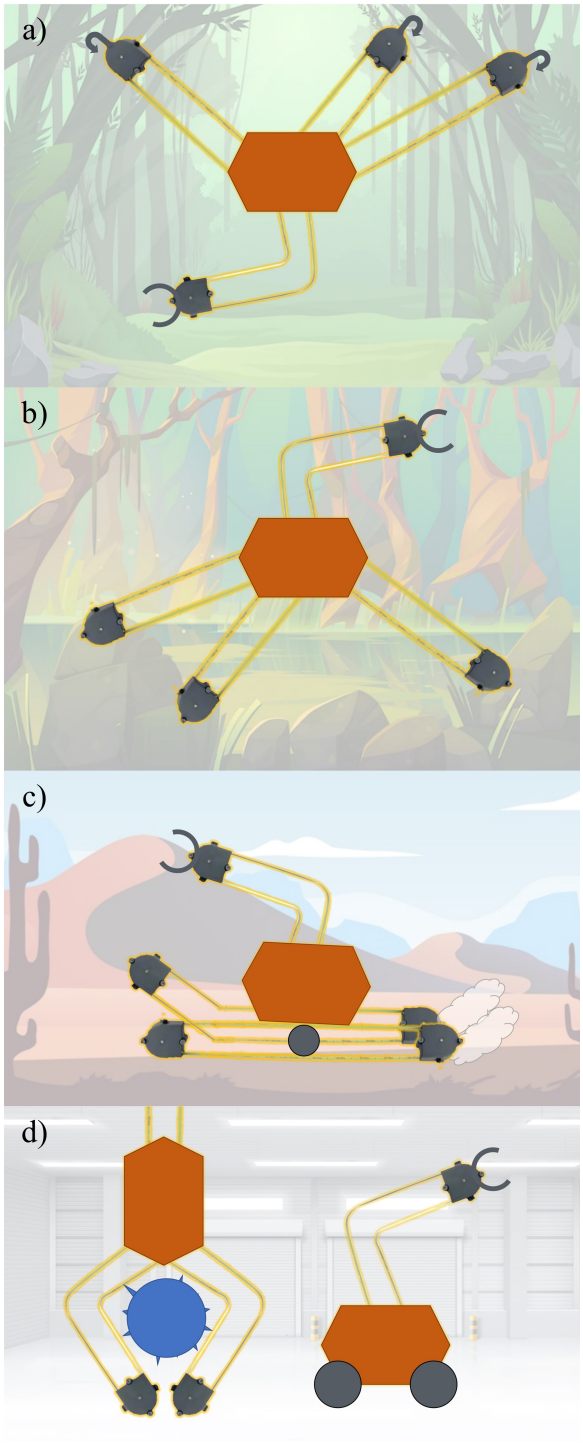

Fig. 19: Concept art of potential EEMMMa configurations. Many concepts have redundant limbs that can be repurposed for inspection or manipulation tasks. a) Suspended robot that deploys anchors to trees. b) Quadruped with telescopic point feet. c) Tread morphing closed-loop tape tank robot. d) Manipulation focused robots.

if a limb is damaged, the system can continue functioning by simply repurposing the remaining limbs.

Beyond climbing robots, there are many other mobility schemes that can be explored. Legged locomotion could use EEMMMa extendable legs for a quadrupedal system, depicted in Fig. 19b. This could be highly advantageous for stepping over obstacles rather than traveling around them. In environments that feature wide-spanning hazards like water and mud, such as swamps, this would make path planning much easier and safer. For manipulation tasks, the quadruped could establish three stable points of contact with the floor and use the fourth limb as a bendable arm for tasks such as reaching submerged objects.

The principles explored in EEMMMa could also be used to improve platforms that focus purely on either mobility or manipulation. EEMMMa's morphability could be used for a closed-loop continuous tape as a tank tread for movement, utilizing the pulley-brake mechanism to morph the shape of the treads to move over obstacles, as seen in Fig. 19c. EEMMMa could also serve as fingers for a compliant gripper that morphs its shape to conform around objects. The tape's steel construction could be favorable for conforming to shapes with sharp corners that could damage other soft robotic shape-morphing manipulators.

The limitations of tape spring limbs can be explored in future work as well. Deploying the limb at long lengths decreases the limb's ability to handle transverse and compressive loads due to increasing moment arms. Longer lengths also increases the limb's sensitivity to external forces and the severity of vibrations, which can limit its usefulness as a manipulator. The presence of gravity greatly affects the characteristics of the limb and can limit deployment in certain directions. Additionally, the maximum length deployable is physically limited by the tape's geometric properties. Finally, while the limb is generally protected from accidents since it can deform elastically, there is risk of plastic deformation if the tape loop gets caught or bent excessively, which would permanently affect its deployment characteristics or cause the limb to be unable to retract. Examining these limitations will help enhance EEMMMa's potential to enable a wide variety of long-reach manipulators and locomotion schemes for future mobile robots.

Acknowledgements

The authors would like to thank the Quan and Hong Families for their constant support and inspiration, as well as Gabriel Fernandez, Colin Togashi, Kyle Gillespie, and Varit Vicathorn for their assistance.

References

[1] Tony Trupp, I. Spider monkeys. [Online; accessed October 10, 2022].

[2] Cant, J. G., 1986. "Locomotion and feeding postures of spider and howling monkeys: field study and evolutionary interpretation". *Folia primatologica,* **46**(1), pp. 1–14.

[3] Carpenter, K. C., Wiltsie, N., and Parness, A., 2016. "Rotary microspine rough surface mobility". *IEEE/ASME Transactions on Mechatronics,* **21**, pp. 2378–2390.

[4] Liu, Y., Sun, S., Wu, X., and Mei, T., 2015. "A wheeled wall-climbing robot with bio-inspired spine

mechanisms". *Journal of Bionic Engineering,* **12**(1), pp. 17–28.

[5] Suzuki, M., Kitai, S., and Hirose, S., 2008. "Basic systematic experiments and new type child unit of anchor climber: Swarm type wall climbing robot system". In 2008 IEEE International Conference on Robotics and Automation, IEEE, pp. 3034–3039.

[6] Asbeck, A. T., Kim, S., Cutkosky, M. R., Provancher, W. R., and Lanzetta, M., 2006. "Scaling hard vertical surfaces with compliant microspine arrays". *The International Journal of Robotics Research,* **25**(12), pp. 1165–1179.

[7] Saunders, A., Goldman, D. I., Full, R. J., and Buehler, M., 2006. "The rise climbing robot: body and leg design". In Unmanned Systems Technology VIII, Vol. 6230, SPIE, pp. 401–413.

[8] Parness, A., Abcouwer, N., Fuller, C., Wiltsie, N., Nash, J., and Kennedy, B., 2017. "Lemur 3: A limbed climbing robot for extreme terrain mobility in space". In 2017 IEEE international conference on robotics and automation (ICRA), IEEE, pp. 5467–5473.

[9] Kalouche, S., Wiltsie, N., Su, H.-J., and Parness, A., 2014. "Inchworm style gecko adhesive climbing robot". In 2014 IEEE/RSJ International Conference on Intelligent Robots and Systems, pp. 2319–2324.

[10] Kawasaki, S., and Kikuchi, K., 2014. "Development of a small legged wall climbing robot with passive suction cups". In The 3rd International Conference on Design Engineering and Science, ICDES, Vol. 2014, pp. 112–116.

[11] Vehar, C., Kota, S., and Dennis, R., 2004. "Closed-loop tape springs as fully compliant mechanisms: preliminary investigations". In International Design Engineering Technical Conferences and Computers and Information in Engineering Conference, Vol. 46954, pp. 1023–1032.

[12] Do, B. H., Osele, O. G., and Okamura, A. M., 2021. "A lightweight, high-extension, planar 3-degree-of-freedom manipulator using pinched bistable tapes". *arXiv preprint arXiv:2110.09751*.

[13] Taffetani, M., Box, F., Neveu, A., and Vella, D., 2019. "Limitations of curvature-induced rigidity: How a curved strip buckles under gravity". *EPL (Europhysics Letters),* **127**(1), p. 14001.

[14] Pini, V., Ruz, J., Kosaka, P. M., Malvar, O., Calleja, M., and Tamayo, J., 2016. "How two-dimensional bending can extraordinarily stiffen thin sheets". *Scientific reports,* **6**(1), pp. 1–6.

[15] Jeon, S., and Murphey, T., 2011. "Design and analysis of a meter-class cubesat boom with a motor-less deployment by bi-stable tape springs". In 52nd AIAA/ASME/ASCE/AHS/ASC Structures, Structural Dynamics and Materials Conference 19th AIAA/ASME/AHS Adaptive Structures Conference 13t, p. 1731.

[16] Seffen, K., You, Z., and Pellegrino, S., 2000. "Folding and deployment of curved tape springs". *International Journal of Mechanical Sciences,* **42**(10), pp. 2055–2073.

[17] Dewalque, F., Collette, J.-P., and Brüls, O., 2016. "Mechanical behaviour of tape springs used in the deployment of reflectors around a solar panel". *Acta Astronautica,* **123**, pp. 271–282.

[18] Gan, W., and Pellegrino, S., 2003. "Closed-loop deployable structures". In 44th AIAA/ASME/ASCE/AHS/ASC Structures, Structural Dynamics, and Materials Conference, p. 1450.

[19] Hong, D. W., Ingram, M., and Lahr, D., 2009. "Whole skin locomotion inspired by amoeboid motility mechanisms".

[20] Seffen, K., and Pellegrino, S., 1999. "Deployment dynamics of tape springs". *Proceedings of the Royal Society of London. Series A: Mathematical, Physical and Engineering Sciences,* **455**(1983), pp. 1003–1048.

[21] Guinot, F., Bourgeois, S., Cochelin, B., and Blanchard, L., 2012. "A planar rod model with flexible thin-walled cross-sections. application to the folding of tape springs". *International Journal of Solids and Structures,* **49**(1), pp. 73–86.

[22] Watt, A. M., and Pellegrino, S., 2002. "Tape-spring rolling hinges". In Proceedings of the 36th Aerospace Mechanisms Symposium, Citeseer, pp. 15–17.

[23] Seffen, K., and Pellegrino, S., 1997. "Deployment of a rigid panel by tape-springs".

[24] Pellegrino, S., Green, C., Guest, S., and Watt, A., 2000. *SAR advanced deployable structure*. University of Cambridge, Department of Engineering.

[25] Oberst, S., Tuttle, S., Griffin, D., Lambert, A., and Boyce, R., 2018. "Experimental validation of tape springs to be used as thin-walled space structures". *Journal of Sound and Vibration,* **419**, pp. 558–570.

[26] Pellegrino, S., 2015. "Folding and deployment of thin shell structures". In *Extremely deformable structures*. Springer, pp. 179–267.

[27] Spenko, M. J., Haynes, G. C., Saunders, J., Cutkosky, M. R., Rizzi, A. A., Full, R. J., and Koditschek, D. E., 2008. "Biologically inspired climbing with a hexapedal robot". *Journal of field robotics,* **25**(4-5), pp. 223–242.

[28] Pedivellano, A., and Pellegrino, S., 2019. "Stability analysis of coiled tape springs". In AIAA Scitech 2019 Forum, p. 1523.

[29] Lynch, G. A., Clark, J. E., Lin, P.-C., and Koditschek, D. E., 2012. "A bioinspired dynamical vertical climbing robot". *The International Journal of Robotics Research,* **31**(8), pp. 974–996.

[30] Mansfield, E. H., 1973. "Large-deflexion torsion and flexure of initially curved strips". *Proceedings of the Royal Society of London. A. Mathematical and Physical Sciences,* **334**(1598), pp. 279–298.

A Summary Video

Link: https://www.youtube.com/watch?v=Ou8liYu03RA